

Optimizing stress resistance in MEMS inertial sensors through material and thickness variations

Miladina Rizka Aziza¹, Onny Setyawati², Jumiadi³

¹Department of Electrical Engineering, Universitas Islam Negeri Maulana Malik Ibrahim Malang, Malang, Indonesia

²Department of Electrical Engineering, Brawijaya University, Malang, Indonesia

³Department of Mechanical Engineering, Universitas Merdeka Malang, Malang, Indonesia

Article Info

Article history:

Received Jul 26, 2024

Revised Feb 27, 2025

Accepted Mar 26, 2025

Keywords:

Inertial sensor

Material

MEMS

Thickness

Von mises stress

ABSTRACT

Stress on the micro-electromechanical system (MEMS) sensors significantly decreases sensor accuracy. Thermomechanical stresses induced by the packaging assembly process and external loads during operation induce a shift in the output signal (offset) of MEMS sensors. To achieve high precision in accelerometers, gyroscopes, and other MEMS devices, it is crucial to employ advanced modeling and simulation techniques to mitigate stress-induced offset drift. Therefore, this paper aims to explore and simulate stress on inertial sensors by designing a gyroscope tuning fork with a perforated proof mass to reduce the damping effect. Our findings provide insights for decreasing stress by varying the material and thickness of the inertial sensor. The least stress was obtained from an inertial silicon sensor with 5 and 20 mm thicknesses.

This is an open access article under the [CC BY-SA](https://creativecommons.org/licenses/by-sa/4.0/) license.



Corresponding Author:

Miladina Rizka Aziza

Department of Electrical Engineering, Universitas Islam Negeri Maulana Malik Ibrahim Malang

65144, Malang, Indonesia

Email: miladinarizka@uin-malang.ac.id

1. INTRODUCTION

The development of micro-electromechanical system (MEMS) technology has introduced numerous new consumer and industrial applications, with inertial measurement being one of its most crucial application areas [1], [2]. An inertial sensor serves as device that can measure inertia, which generally consist of two types, accelerometers which is used to detect the exact magnitude of direction and acceleration (or g-force), and gyroscopes which is used to measure angular speed [3]. Basically, accelerometer and gyroscope can be modeled as a system consisted of a proof mass, spring and damper [4]. Capacitive accelerometer with perforated proof mass structure has been widely used because it reduces air attenuation and significantly improves sensor performance [5]-[7]. Vibrations of mechanical elements which is also formed in proof mass are utilized by gyroscopes to detect rotation.

MEMS gyroscopes are classified into several structures, such as gimbal gyroscopes, tuning fork gyroscopes, vibrating ring gyroscopes, and solid-state gyroscopes [8]. Among these, tuning fork gyroscopes are mostly favored due to their superior performance, which is attributed to their planar structure facilitating large-scale manufacturing, effective common-mode rejection, and low power consumption [9]-[11]. However, achieving high sensitivity in tuning fork gyroscopes remains a significant challenge for optimal performance [12], [13].

Inertial sensors have been widely employed to deliver precise position and motion measurement solution across numerous key sectors, such as aerospace, robotics, healthcare, power electronics, neurotechnologies and portable devices [14]-[19]. The diversity of these applications results in different requirements on inertial sensors regarding accuracy, size, power consumption, and cost [20]. With the

increasing demand in MEMS technology, it is crucial to consider various factors affecting MEMS device performance, such as surface tension, viscosity, squeeze film damping, and residual stress [21].

Stress on micro-electromechanical systems (MEMS) sensors can lead to reduced sensor accuracy [21], [22]. MEMS sensors might undergo a shift in the output signal (offset) due to thermomechanical stresses caused by the packaging assembly process and external loads applied during operation [23], [24]. Modeling and simulation to minimize stress-induced offset drift is critical to achieving high precision in accelerometers, gyroscopes, and other MEMS devices [25]. Although thermomechanical stress is known as the source of error in MEMS devices, the role of material and thickness variations in enhancing MEMS device performances is not fully explored. This research aims to address the challenges by focusing on the stress behavior in tuning fork gyroscopes inertial sensors. Specifically, it simulates and analyzes how material properties and sensor dimensions affect stress distribution, with the goal of minimizing stress-induced errors. By optimizing the design, particularly with the inclusion of a perforated proof mass to reduce damping, this study contributes to enhancing the precision and reliability of MEMS sensors used across various industries.

2. METHOD

2.1. Device design

Figure 1 illustrates the process of developing inertial sensor. The primary component of the inertial sensor consists of three parts: the proof mass, the hole, and the arm, as shown in Figure 1(a). Table 1 demonstrates the structural dimensions of the inertial sensor. The total dimensions of this device are 150 in length, 190 mm in width, and 10 mm in height. The device was designed using FreeCAD software, then imported into Salome software to generate mesh. The design was categorized into several groups: GroupGFix, GroupGTop, GroupGothers, and Group_all, as shown in Figure 1(b). GroupGFix, shown in orange, represents the stationary part of the sensor. GroupGTop, shown in blue, represents the part of the sensor where stress will be exerted. Meanwhile, the GroupGothers, shown in green, are groups other than GroupGFix and GroupGTop. Once the mesh was created, all parts are grouped.

Table 1. Structural dimensions of inertial sensor

Sensor structure	Length×Width×Height (mm)
Box (Proof Mass)	150×150×10
Hole box	6×6×10
Arm	145×20×10

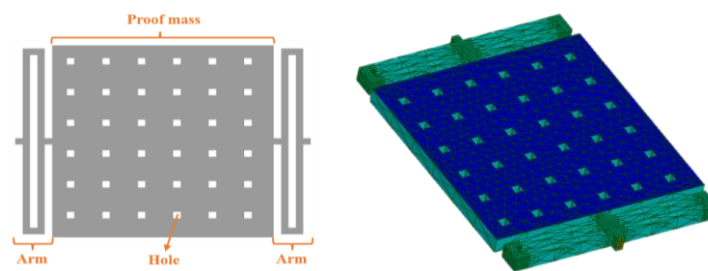


Figure 1. The design of inertial sensor: (a) inertial sensor structure and (b) the mesh creation using salome

2.2. Simulation method

ElmerGUI is an open-source finite element software designed for multi-physical problems. This software serves to provide treatment to inertial sensors. Figure 2 presents the design and meshing process carried out in ElmerGUI, which corresponds to the mesh generation conducted in Salome software. Figure 2(a) illustrates the meshing of the sensor's structural design, detailing various boundary groups: GroupGTop represents the top and bottom part of inertia sensor, where stress will be exerted Figure 2(b), GroupGothers include all regions except the top and bottom parts Figure 2(c), Group_all represents the entire sensor Figure 2(d), and GroupGFix correspond to fixed area of the inertia sensor that remain stationary Figures 2(e) and 2(f). The linear elasticity equation was set to calculate the stress value on the object. The equation setting is shown in Table 2, the value of stress body force was formulated in (1), and thus, the body force applied on the object is expressed in (2). The material used for the inertial sensor was silicon. The parameters used for silicon materials are shown in Table 3. In order to arrange the object surface that will be treated, the boundary condition need to be set.

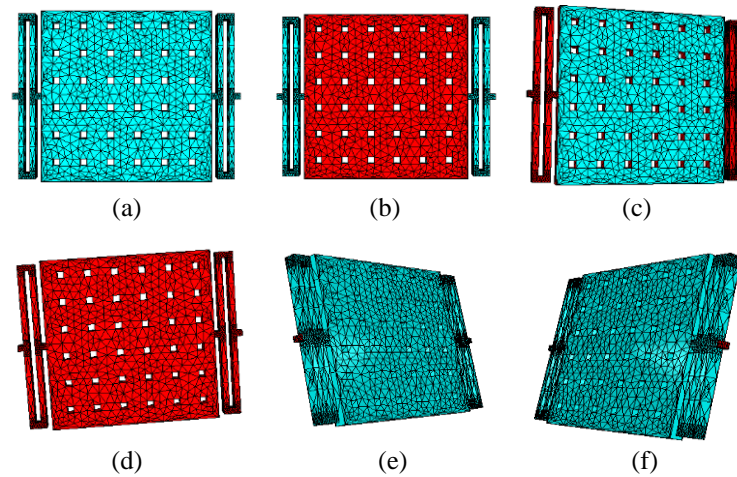


Figure 2. The design of the inertia sensor and meshing group: (a) the complete structure of the inertia sensor (b) boundary GroupGTop, (c) boundary GroupGothers, (d) group_all, and (e)-(f) boundary GroupGFix

Table 2. Equation setting in ElmerGUI software

Equation Configuration in ElmerGUI	
Solver 1	
Equation = Linear elasticity	
Procedure = "StressSolve" "StressSolver"	
Variable = -dofs 3 Displacement	
Calculate Loads = True	
Calculate Stresses = True	
Exec Solver = Always	
Stabilize = False	
Bubbles = False	
Lumped Mass Matrix = False	
Optimize Bandwidth = True	
Steady State Convergence Tolerance = 1.0e-6	
Nonlinear System Convergence Tolerance = 1.0e-7	
Nonlinear System Max Iterations = 1	
Nonlinear System Newton After Iterations = 3	
Nonlinear System Newton After Tolerance = 1.0e-3	
Nonlinear System Relaxation Factor = 1	
Linear System Solver = Iterative	
Linear System Iterative Method = CG	
Linear System Max Iterations = 200	
Linear System Convergence Tolerance = 1.0e-6	
Linear System Preconditioning = ILU0	
Linear System ILUT Tolerance = 1.0e-3	
Linear System Abort Not Converged = False	
Linear System Residual Output = 1	
Linear System Precondition Recompute = 1	
End	

Table 3. Material parameter

Material	Parameter	Value
Silicon	Density	2.330 g/cm ³
	Youngs modulus	190 Gpa
	Poisson ratio	0.27
	Stress body force	$2.2834 \times 10^{-8} \mu\text{N}/\mu\text{m}^3$
Germanium	Density	5.323 g/cm ³
	Youngs modulus	103 Gpa
	Poisson ratio	0.26
	Stress body force	$5.2165 \times 10^{-8} \mu\text{N}/\mu\text{m}^3$
Galium Arsenide	Density	5.318 g/cm ³
	Youngs modulus	85.5 GPa
	Poisson ratio	0.31
	Stress body force	$5.2136 \times 10^{-8} \mu\text{N}/\mu\text{m}^3$

The value of stress body force was in (1).

$$\text{Stress Body Force} = \text{Gravity Force} \times \text{Density} \quad (1)$$

Thus, the body force applied to the object is expressed in the (2):

$$\begin{aligned} \text{Stress Body Force} &= 9.8 \, \text{m/s}^2 \times 2330 \, \text{kg/m}^3 \\ \text{Stress Body Force} &= 22834 \, \text{kg/s}^2 \text{m}^2 \end{aligned} \quad (2)$$

Because the stress input was influenced by gravitational forces, the value of volume forces was applied to the z-axis. The negative sign indicates the opposite direction. The pressure was set to 0 which indicates no isotropic pressure on the body sensor.

3. RESULTS AND DISCUSSION

Von Mises stress is the stress level that leads to material failure when the material experiences triaxial stress which produces strain energy. Failure occurs when the strain energy from the triaxial stress is equal to the strain energy observed in a standard tensile test of the material's yield point. Basically, stress is defined as the force exerted per unit area, as shown in (3).

$$\sigma = C \frac{Pl^2}{h^2} \quad (3)$$

σ : stress

C: constant

P: pressure

l: structure length

h: structure thickness

The linear elasticity equation can be used to determine the stress generated within an object. Elmer software provides a graphic user interface (GUI) that allows users to view desired responses and capable of demonstrating the solution of linear elasticity equation on a 3D object. In this case, the 3D object is an inertial sensor commonly used in MEMS sensors. Mathematically, the stress equation can be described in (4) and (5).

$$\tau^{ij} = C^{ijkl} \varepsilon_{kl} - \beta^{ij} (T - T_o) \quad (4)$$

$$\tau(u) = \lambda (\nabla \cdot u) I + \mu (\nabla \cdot u + (\nabla \cdot u)^T) \quad (5)$$

where ε is the strain and C is the elastic modulus. The parameters to be considered in the material selection are density, Young's modulus, and Poisson Ratio.

$$\lambda = \frac{Y\kappa}{(1+\kappa)(1-2\kappa)} \quad (6)$$

$$\mu = \frac{Y}{2(1+\kappa)} \quad (7)$$

where Y is Young's modulus, κ is Poisson's ratio, λ and μ are material forming parameters.

Based on the (6) and (7), it is evident that the stress level can be affected by both the type of material and the thickness of different structures. Therefore, this paper will discuss how the material and thickness of the inertial sensor impact the resulting stress.

According to simulation results using Elmer software, the maximum stress value (in red) was 9.35×10^{-4} MPa, the optimal stress value (in green) was 4.68×10^{-4} MPa, and the minimum stress was (in blue) 7.47×10^{-7} MPa, as shown in Table 4. Simulation results demonstrate in Figure 3 that the stress part was on the arm. Once a force is applied to the sensor, displacement occurs and stress appears in the sensor. Since the portion of the sensor that remains stationary is in the sensor arm, stress also appears in the sensor arm, as shown in Figure 3(a). This occurs because the sensor arms experienced tension to prevent movement. Moreover, the stress was concentrated at the ends of the sensor arm due to the fact that the smaller the cross-sectional area, the greater the stress experienced. Figure 3(b) illustrates the convergence graph of simulation results, it can be seen that to reach the linear state it takes up to the 6th iteration.

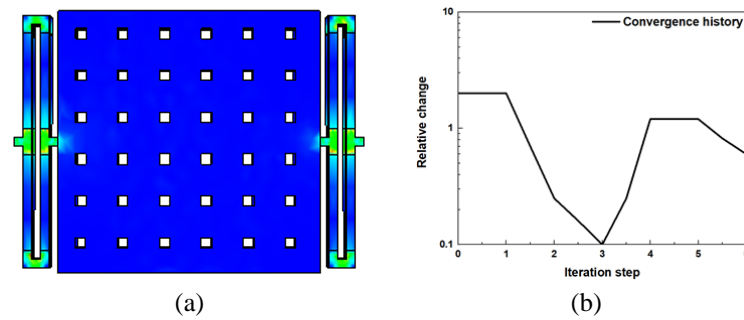


Figure 3. Von Mises stress simulation of: (a) inertial sensor at 10 mm thickness and (b) convergence history of silicon inertial sensor

3.1. Material modification simulation

In inertial sensors, the material used is the key factor that affects stress. Therefore, we tried to simulate the inertial sensor using different materials, as shown in Figure 4. The von Mises stress simulation results for different materials used in the sensor structure highlight the specific material stress distribution that is concentrated in the sensor arms, as illustrated in Figures 4(a)-(c), respectively, for silicon, germanium, and gallium arsenide. Table 4 and Figure 4(d) demonstrates the simulation results of material modification. The minimum stress of silicon, germanium, and gallium arsenide were 7.47×10^{-7} , 2.41×10^{-6} , and 2.50×10^{-6} MPa, respectively. Meanwhile, the maximum stress of silicon, germanium, and gallium arsenide were 9.35×10^{-4} , 2.23×10^{-3} , and 2.02×10^{-3} MPa, respectively. The higher material density leads to greater stress, resulting in an increase in von Mises stress. Thus, the stress produced by germanium was greater than gallium arsenide and silicon, which was in accordance with (6) and (7).

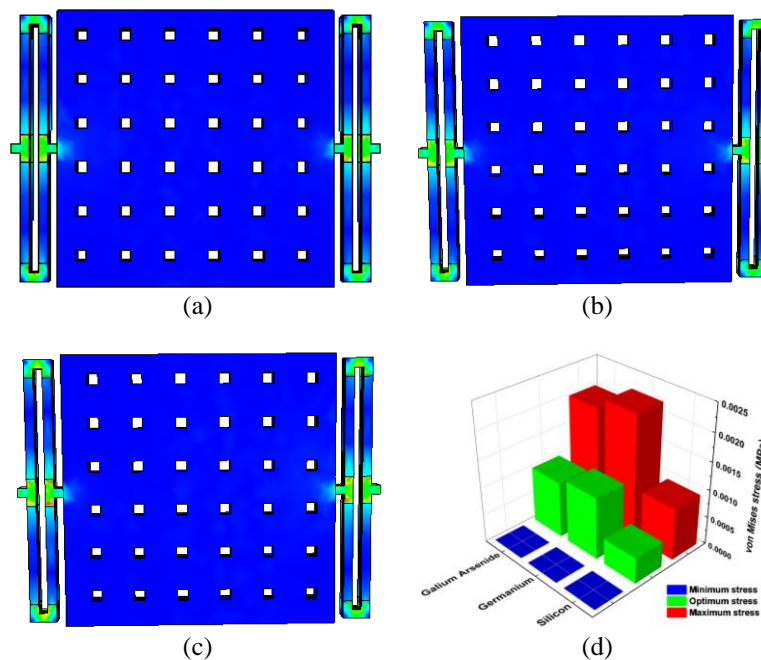


Figure 4. Von Mises stress simulation of: (a) silicon, (b) germanium, (c) gallium arsenide, and (d) graph of von Mises stress with different materials

Table 4. Simulation results of inertial sensor with material modification

Material	Minimum stress Blue (MPa)	Optimum stress Green (MPa)	Maximum stress Red (MPa)
Silicon	7.47×10^{-7}	4.68×10^{-4}	9.35×10^{-4}
Germanium	2.41×10^{-6}	1.12×10^{-3}	2.23×10^{-3}
Gallium Arsenide	2.50×10^{-6}	1.01×10^{-3}	2.02×10^{-3}

3.2. Thickness modification simulation

Besides the material used, the length and thickness of the structure can also impact the stress produced by the inertial sensor. In this research, we adjusted the thickness of the sensor while keeping the other dimensions constant. Figure 5 presents the von Mises stress simulations using various thicknesses, highlighting the effect of thickness on stress distribution. Figure 5(a)-(e) illustrates the von Mises stress distribution with different thicknesses of 5, 7, 10, 15, and 20 mm, respectively. As the sensor's thickness increases, the minimum stress value (shown in blue) decreases, which aligns with the formula in (3). For the optimal (shown in green) and maximum (shown in red) stress, at thicknesses of 10, 15, and 20 mm, greater thickness results in higher stress values. However, at 5 and 7 mm thicknesses, the optimal and maximum stress values deviate from the formula.

The minimum stress of thickness variation were 2.31×10^{-6} , 9.44×10^{-7} , 7.47×10^{-7} , 7.20×10^{-7} , 6.52×10^{-7} MPa, respectively, for 5, 7, 10, 15 and 20 mm. Meanwhile, the maximum stress of thickness variation were 6.12×10^{-4} , 8.87×10^{-4} , 9.35×10^{-4} , 8.11×10^{-4} , 5.26×10^{-4} MPa, respectively, for 5, 7, 10, 15, and 20 mm. The simulation results indicate that at 5 and 7 mm, the distribution of maximum stress values is broader than at 10, 15, and 20 mm, as shown in Table 5 and Figure 5(f). This demonstrates that a thinner sensor leads to a wider distribution of maximum stress, which can impact the sensor's performance.

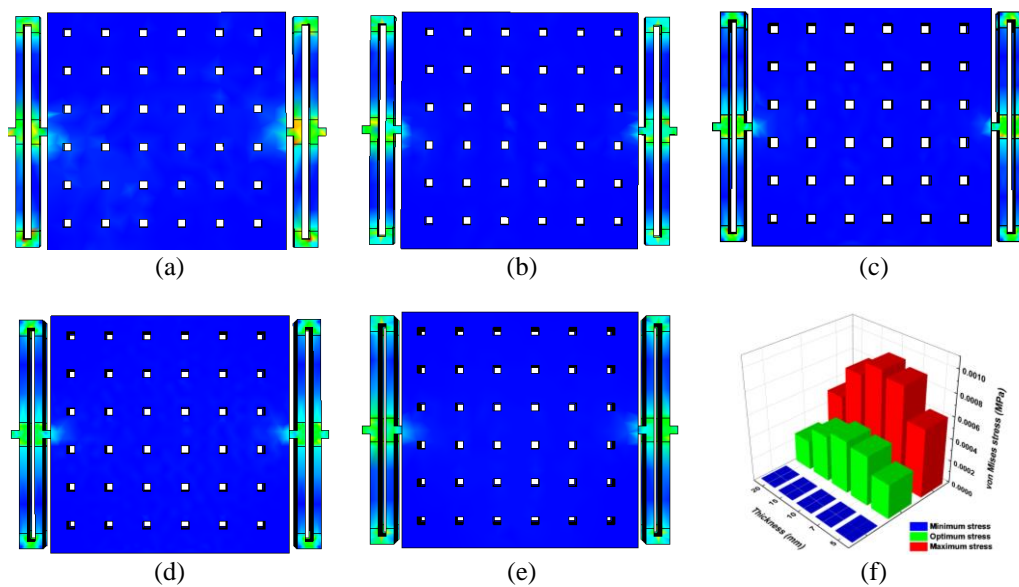


Figure 5. Von Mises stress simulation at: (a) 5 mm, (b) 7 mm, (c) 10 mm, (d) 15, (e) 20 mm thicknesses, and (f) graph of von Mises stress with different thicknesses

Table 5. Simulation results of inertial sensor with thickness modification

Thickness	Minimum stress Blue (MPa)	Optimum stress Green (MPa)	Maximum stress Red (MPa)
5 mm	2.31×10^{-6}	3.07×10^{-4}	6.12×10^{-4}
7 mm	9.44×10^{-7}	4.44×10^{-4}	8.87×10^{-4}
10 mm	7.47×10^{-7}	4.68×10^{-4}	9.35×10^{-4}
15 mm	7.20×10^{-7}	4.06×10^{-4}	8.11×10^{-4}
20 mm	6.52×10^{-7}	2.65×10^{-4}	5.26×10^{-4}

4. CONCLUSION

Stress emerges as a crucial parameter to be considered in MEMS sensors to maintain their accuracy and performance. Our findings provide conclusive evidence that this phenomenon is associated with the material composition and the thickness of the sensor, which influence the level of stress exerted. Recent observations suggest that the higher material density correlates with heightened stress level, thus Germanium has the highest stress level compared to Silicon and Gallium Arsenide. Furthermore, thicker sensor dimensions lead to a reduction in stress level. Inertial sensor with the thickness of 5 and 7 mm have broader distribution of stress values than at 10, 15, and 20 mm thicknesses.

ACKNOWLEDGEMENTS

This work was supported by Universitas Islam Negeri Maulana Malik Ibrahim Malang and Brawijaya University.

FUNDING INFORMATION

Authors state no funding involved.

AUTHOR CONTRIBUTIONS STATEMENT

Name of Author	C	M	So	Va	Fo	I	R	D	O	E	Vi	Su	P	Fu
Miladina Rizka Aziza	✓	✓	✓	✓	✓	✓	✓	✓	✓	✓	✓		✓	✓
Onny Setyawati	✓	✓		✓	✓	✓	✓			✓		✓		
Jumiadi				✓	✓	✓	✓			✓		✓		

C : **C**onceptualization

M : **M**ethodology

So : **S**oftware

Va : **V**alidation

Fo : **F**ormal analysis

I : **I**nvestigation

R : **R**esources

D : **D**ata Curation

O : **O**riting - **O**riginal Draft

E : **E**riting - **R**eview & **E**editing

Vi : **V**isualization

Su : **S**upervision

P : **P**roject administration

Fu : **F**unding acquisition

CONFLICT OF INTEREST STATEMENT

Authors state no conflict of interest.

DATA AVAILABILITY

Data availability is not applicable to this paper as no new data were created or analyzed in this study.




REFERENCES

- [1] D. K. Shaeffer, "MEMS inertial sensors: a tutorial overview," *IEEE Communications Magazine*, vol. 51, no. 4, pp. 100-109, 2013, doi: 10.1109/MCOM.2013.6495768.
- [2] Y. Xu *et al.*, "Reliability of MEMS inertial devices in mechanical and thermal environments: a review," *Heliyon*, vol. 10, no. 5, pp. e27481, 2024/03/15/ 2024, doi: 10.1016/j.heliyon.2024.e27481.
- [3] A. Colagrossi, V. Pesce, S. Silvestrini, D. Gonzalez-Arjona, P. Hermosin, and M. Battilana, "Chapter six - sensors," in *Modern Spacecraft Guidance, Navigation, and Control*, V. Pesce, A. Colagrossi, and S. Silvestrini, Eds.: Elsevier, 2023, pp. 253-336, doi: 10.1016/B978-0-323-90916-7.00006-8.
- [4] S. Veena, N. Rai, H. L. Suresh, and V. S. Nagaraja, "Design, modelling, and simulation analysis of a single Axis MEMS-based capacitive accelerometer," *ArXiv*, vol. 69, no. 10, pp. 82-88, 2021, doi: 10.48550/arXiv.2111.03816.
- [5] G. A. Khouqeer, S. Suganthi, N. Alanazi, A. Alodhayb, M. Muthuramamoorthy, and S. Pandiaraj, "Design of MEMS capacitive comb accelerometer with perforated proof mass for seismic applications," *Journal of King Saud University - Science*, vol. 35, no. 3, p. 102560, 2023, doi: 10.1016/j.jksus.2023.102560.
- [6] Y. Kamada, A. Isobe, T. Oshima, Y. Furubayashi, T. Ido, and T. Sekiguchi, "Capacitive MEMS accelerometer with perforated and electrically separated mass structure for low noise and low power," *Journal of Microelectromechanical Systems*, vol. 28, no. 3, pp. 401-408, 2019, doi: 10.1109/JMEMS.2019.2903349.
- [7] S. Veena, N. Rai, A. M. R. Morey, H. L. Suresh, and H. Shaik, "Design and simulation of MEMS based capacitive accelerometer," Singapore, 2022: Springer Singapore, vol. 2, no. 12, pp. 207-223, doi: 10.1007/978-981-16-2919-8_19.
- [8] K. Liu *et al.*, "The development of micro-gyroscope technology," *Journal of Micromechanics and Microengineering*, vol. 19, no. 11, p. 113001, 2009/10/16 2009, doi: 10.1088/0960-1317/19/11/113001.
- [9] M. N. Nguyen, N. S. Ha, L. Q. Nguyen, H. M. Chu, and H. N. Vu, "Z-Axis micromachined tuning fork gyroscope with low air damping," *Micromachines*, vol. 8, no. 2, pp. 1-10, 2017, doi: 10.3390/mi8020042.
- [10] M. S. Weinberg and A. Kourepenis, "Error sources in in-plane silicon tuning-fork MEMS gyroscopes," *Journal of Microelectromechanical Systems*, vol. 15, no. 3, pp. 479-491, 2006, doi: 10.1109/JMEMS.2006.876779.
- [11] R. Wang, P. Cheng, F. Xie, D. Young, and Z. Hao, "A multiple-beam tuning-fork gyroscope with high quality factors," *Sensors and Actuators A: Physical*, vol. 166, no. 1, pp. 22-33, 2011, doi: 10.1016/j.sna.2010.12.024.
- [12] Z. Li, S. Gao, L. Jin, H. Liu, Y. Guan, and S. Peng, "Design and mechanical sensitivity analysis of a MEMS tuning fork gyroscope with an anchored leverage mechanism," *Sensors*, vol. 19, no. 16, pp. 1-19, 2019, doi: 10.3390/s19163455.
- [13] C. Xiong *et al.*, "Design and optimization of a novel MEMS tuning fork gyroscope microstructure," (in eng), *Micromachines (Basel)*, vol. 13, no. 2, pp. 1-14, 2022, doi: 10.3390/mi13020172.
- [14] X. Ru, N. Gu, H. Shang, and H. Zhang, "MEMS inertial sensor calibration technology: current status and future trends," *Micromachines*, vol. 13, no. 6, 2022, doi: 10.3390/mi13060879.




- [15] N. El-Sheimy and A. Youssef, "Inertial sensors technologies for navigation applications: state of the art and future trends," *Satellite Navigation*, vol. 1, no. 1, p. 2, 2020, doi: 10.1186/s43020-019-0001-5.
- [16] M. Fennel, L. Driller, A. Zea, and U. D. Hanebeck, "Observability-based placement of inertial sensors on robotic manipulators for kinematic state estimation," *IFAC-PapersOnLine*, vol. 56, no. 2, pp. 5293-5299, 2023, doi: 10.1016/j.ifacol.2023.10.171.
- [17] F. Coito, A. Eleutério, S. Valtchev, and F. Coito, "Tracking a mobile robot position using vision and inertial sensor," Berlin, Heidelberg, 2014: Springer Berlin Heidelberg, vol. 423, pp. 201-208, 2014, doi: 10.1007/978-3-642-54734-8_23.
- [18] S. Sun *et al.*, "MEMS ultrasonic transducers for safe, low-power and portable eye-blinking monitoring," *Microsystems & Nanoengineering*, vol. 8, no. 1, p. 63, 2022, doi: 10.1038/s41378-022-00396-w.
- [19] H. T. Le *et al.*, "MEMS inductor fabrication and emerging applications in power electronics and neurotechnologies," *Microsystems & Nanoengineering*, vol. 7, no. 1, p. 59, 2021, doi: 10.1038/s41378-021-00275-w.
- [20] J. Collin, P. Davidson, M. Kirkko-Jaakkola, and H. Leppäkoski, "Inertial sensors and their applications," in *Handbook of Signal Processing Systems*, S. S. Bhattacharyya, E. F. Deprettere, R. Leupers, and J. Takala, Eds. Cham: Springer International Publishing, 2019, pp. 51-85, doi: 10.1007/978-3-319-91734-4_2.
- [21] S. Dutta and A. Pandey, "Overview of residual stress in MEMS structures: its origin, measurement, and control," *Journal of Materials Science: Materials in Electronics*, vol. 32, no. 6, pp. 6705-6741, 2021, doi: 10.1007/s10854-021-05405-8.
- [22] G. Boldeiu, D. Vasilache, V. Moagar, A. Stefanescu, and G. Ciuprina, "Study of the von Mises stress in RF MEMS switch anchors," in *2015 International Semiconductor Conference (CAS)*, 2015, pp. 219-222, doi: 10.1109/SMICND.2015.7355213.
- [23] X. Zhang, S. Park, and M. W. Judy, "Accurate assessment of packaging stress effects on MEMS sensors by measurement and sensor-package interaction simulations," *Journal of Microelectromechanical Systems*, vol. 16, no. 3, pp. 639-649, 2007, doi: 10.1109/JMEMS.2007.897088.
- [24] M. Hosseini-Pishrobat, D. Erkan, and E. Tatar, "Analytical and experimental study of stress effects in a MEMS ring gyroscope," *Sensors and Actuators A: Physical*, vol. 362, p. 114639, 2023, doi: 10.1016/j.sna.2023.114639.
- [25] X. Han *et al.*, "Advances in high-performance MEMS pressure sensors: design, fabrication, and packaging," *Microsystems & Nanoengineering*, vol. 9, no. 1, p. 156, 2023, doi: 10.1038/s41378-023-00620-1.

BIOGRAPHIES OF AUTHORS






Miladina Rizka Aziza    is a Lecturer in the Department of Electrical Engineering, Universitas Islam Negeri Maulana Malik Ibrahim Malang, Indonesia. She received a Bachelor's degree in Electrical Engineering Department, Brawijaya University in 2018. She got a master's degree in International Curriculum for Advanced Materials Program (iCAMP), National Cheng Kung University, Taiwan, in 2020. Her specialization is organic materials, renewable energy, and skyrmion. Her research areas are two-dimensional materials for water splitting and spintronics application. She can be contacted at email: miladinarizka@uin-malang.ac.id.



Onny Setyawati    is a Lecturer in the Department of Electrical Engineering, Brawijaya University, Indonesia. She received a bachelor's degree in the Electrical Engineering Department from Universitas Gadjah Mada, and a master's degree from Institut Teknologi Bandung and the University of Kassel in Germany. Then she continued her Ph.D. in the same university, the University of Kassel. Her research areas are nanotechnology, photonics, and optical engineering. She is the head of the Electronics Laboratory in the Department of Electrical Engineering, at Brawijaya University. She can be contacted at email: osetyawati@ub.ac.id.



Jumiadi    is a Lecturer in the Department of Mechanical Engineering, Universitas Merdeka Malang, Indonesia. He received Bachelor's degree in Mechanical Engineering Department from Universitas Merdeka Malang in 1988. He got a Master's degree in Metallurgy Engineering, Universitas Indonesia in 2003 with a specialization in metal testing and analysis. His research areas are hardness and microstructure, friction welding, renewable energy, and corrosion. He is the head of the metal testing Lab in the Department of Mechanical Engineering, Universitas Merdeka Malang. He can be contacted at email: jumiadi@unmer.ac.id.